Proceedings of the 23rd National Heat and Mass Transfer Conference and
1st International ISHMT-ASTFE Heat and Mass Transfer Conference
IHMTC2015
17-20 December, 2015, Thiruvananthapuram, India

Paper No. IHMTC2015- 350

COMPUTATIONAL STUDY OF HEAT TRANSFER ENHANCEMENT THROUGH BROKEN AND CONTINUOUS ATTACHED RIBS IN A SQUARE CHANNEL

Anuj Kumar Shukla
Department of Applied Mechanics
Indian Institute of Technology Delhi
anujshukla.cest@gmail.com

Anupam Dewan
Department of Applied Mechanics
Indian Institute of Technology Delhi
adewan@am.iitd.ac.in

ABSTRACT

A computational study was carried out for the heat transfer augmentation in a three-dimensional square channel fitted with different types of ribs. Three RANS based turbulence models were used, namely, the standard k-ε model, RNG k-ε model and realizable k-ε model and the predictions were compared with the reported experimental data. Four rib configurations were used: (a) 90^0 continuous attached ribs, (b) 90^0 continuous detached ribs, (c) 90^0 broken attached thick ribs and (d) 90^0 broken attached thin ribs. The effects of the blockage ratio and rib thickness were investigated for 90^0 broken ribs with Re = 10,000 - 30,000 and p/e (rib pitch) = 10. Broken 90^0 attached ribs with blockage ratios (e/d) of 0.15, 0.10 and 0.08125 were used in order to study the effect of blockage ratio on heat transfer augmentation. For each blockage ratio two rib configurations were used, i.e., thick ribs and thin ribs. We observed that the standard k-ε model provides better results compared to other turbulence models considered. It was observed that thin ribs perform better than thick ribs. Broken rib produced higher levels of turbulence over the heated surface due to better mixing of flow. The average Nusselt number was found to be more at each Reynolds number in case of broken attached ribs as compared to continuous attached ribs.

Keywords: *heat transfer enhancement, turbulent flow, ribbed channel, broken ribs, CFD*

NOMENCLATURE

c	Clearance between rib and wall (m)
d	Hydraulic diameter (m)
e	Rib height (m)
h	Heat transfer coefficient (W/m^2K)
k	Turbulent kinetic energy (m^2/s^2)
Nu	Local Nusselt number (hd/k)
Nu_0	Nusselt number obtained by Dittus and Boelter correlation
Nu_{av}	Area average Nusselt number
P	Mean pressure (Pa)
p	Rib pitch (m)
Pr	Prandtl number
Re	Reynolds number
s	Rib thickness (m)
T	Mean temperature (K)
U	Mean velocity (m/s)

Subscripts and abbreviations

i,j,k	Tensor notation
b,w	Bulk, wall
t	Turbulent quantities
RNG	Re-normalization group

INTRODUCTION

Ribs and rough surfaces are used to enhance heat transfer in any closed channel flow which involves complex flow fields. Researchers have employed many strategies to improve the heat transfer in a channel. But the use of ribs is one of the most employed methods to enhance the rate of heat transfer in a channel. Ribs break the viscous sub-layer due to the flow separation and reattachments in the near wall region. Vortices are generated in the upstream direction from the reattachment point which increases the turbulent kinetic energy. Due to the presence of ribs a secondary flow induces in the square channel. Increase in turbulent kinetic energy and development of secondary flow lead to heat transfer increase in a square channel with the use of ribs [1]. Ribs as a turbulent promoters have been used for many years to enhance the heat transfer in several applications, such as, heat exchangers, internal cooling of a gas turbine blades, turbo machines and nuclear reactors, etc. A large number of papers exist in the literature dealing with heat transfer characteristics of rib fitted channel.

Webb *et al.* [2] concluded that the heat transfer and friction correlations may be extended to a wider range of blockage ratios *(e/d)* by the virtue of the law of the wall similarity. Han *et al.* [3] experimentally showed that ribs with 45º angle of attack have high heat transfer performance than that of 90º angle of attack. Sparrow and Cur [4] observed that the flow separation at the inlet plays an important role in the axial distribution of heat transfer coefficient in the thermal entrance region. Han [5] studied the heat transfer and friction in channels with two opposite rib roughened walls. Han and Spark [1] investigated the effect of rib angle and aspect ratio of the channel on the heat transfer distribution in a rectangular channel.

Han *et al.* [6] showed that the V-shaped ribs provide superior performance than parallel and crossed ribs. They also reported lowest heat transfer with crossed ribs. Lau *et al.* [7] studied the effect of V-shaped ribs array on turbulent heat transfer and friction of fully developed flow in a square channel. They reported that the 60^0 V-shaped ribs with $p/e = 10$ have the highest heat transfer rate as compared to 45^0, 125^0, 135^0 ribs. Han and Zhang [8] showed that the 60^0 parallel broken ribs and 60^0 V-shaped broken ribs provide a higher heat transfer augmentation than the 45^0 parallel and V-shaped ribs. Liou and Wang [9] experimentally observed that the 20% enhancement of heat transfer occurred in a detached rib configuration as compared to attached rib. Rau *et al.* [10] observed that the enhancement of heat transfer occurs due to the development of strong secondary flows. Gao and Sunden [11] showed that V-ribs pointing downstream provided good thermal performance for *Re* ranging from 1000 to 6000.

Chandra *et al*. [12] performed experiments on heat transfer and friction behavior in rectangular channel with varying number of ribbed walls. They observed that the channel with two opposite ribbed walls showed 6% increase in heat transfer over channel with one ribbed wall. Tanda [13] performed experiment and concluded that the features of inter–rib distributions on the heat transfer coefficient are strongly related to the rib shape and geometry. Sewall *et al.* [14] experimentally validated LES results of flow and heat transfer in a stationary ribbed duct. Chang *et al.* [15] observed that as the channel height increases the value of averaged Nusselt number decreases. They observed that LES produces the results within 10-15% of experimental results. Eiamsa-ard and Promvonge [16] observed that due to the recirculation flow, enhancement of heat transfer occurs in a channel. Gupta *et al*. [17] observed that 60º broken ribs provided high heat transfer than 90º continuous ribs.

SriHarsha *et al.* [18] experimentally observed that the heat transfer in a square channel with 60^0 V-broken ribs was higher than that of 90^0 continuous attached ribs. Tanda [19] studied the effect of rib spacing on heat transfer and friction in rectangular channel with 45^0 angled rib turbulators on one and two walls. Promvonge *et al.* [20] numerically studied heat transfer characteristics of turbulent square duct flow through inline V-shaped discrete ribs. They showed that if the test duct is sufficiently large then the duct flow can be considered as the fully developed periodic flow. Smulsky *et al.* [21] observed that as the angle of rib orientation relative to the flow direction decreases, the attachment area, pressure and heat transfer maxima move towards the rib. The local heat transfer for 50º ribs was approximately 40% higher than that of the 90º ribs. Tang and Zhu [22] observed a low value of the local heat transfer just behind the rib due to flow separation and concluded that a rise in the Nusselt number is due to the development of longitudinal vortices generated by inclined broken ribs.

It is clear from the above-mentioned literature review that continuous attached thick ribs have been studied by most researchers for heat transfer augmentation. A limited literature exists dealing with numerical investigations of broken attached ribs, detached ribs and thin ribs for heat transfer enhancement. The objectives of the present study are:

- To gain physical understanding of flow field and heat transfer characteristics of rib roughened square channel;
- To study the effect of detached and broken ribs on heat transfer;
- To study of local heat transfer and average heat transfer in rib roughened square channel;
- To study the effect of various geometric parameters of channel and ribs on heat transfer augmentation;
- To study the effect of thick and thin ribs on heat transfer augmentation.

PHYSICAL GEOMETRY AND BOUNDARY CONDITIONS

A horizontal square duct of cross section 0.04 m x 0.04 m fitted with different types of rib was considered. Promvonge *et al*. [20] observed that if the test duct is sufficiently large then the duct flow can be considered as the fully developed periodic flow. Therefore we have considered periodic domain in the present study. A constant mass flow rate of air with the inlet temperature of 300 *K* was considered in the direction of flow. The air flowed over the inline 90^0 continuous and broken ribs. The flow was considered to be periodic, three-dimensional, fully developed turbulent and incompressible. We have assumed the physical properties of the air to be constant at the initial air temperature. The no slip boundary condition was used over the duct walls as well as on the rib surfaces with the enhanced wall treatment to model turbulence in the vicinity of a solid wall. A constant heat flux of 2500 $W/m^2$was applied at the two opposite vertical heated walls of the square duct and ribs were considered adiabatic [18]. Fig. 1 shows different rib configurations considered in the present study. Continuous 90^0ribs had thickness of 3 mm. For 90^0 broken ribs the non-dimensional thickness (*s/d* of thick ribs was 0.075 and the non-dimensional thickness (*s/d*) of thin ribs was 0.0125.

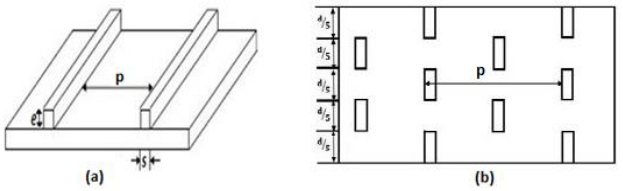


FIGURE 1. Different rib configurations for (a) 90^0 attached rib; (b) 90^0 broken ribs.

The two heated walls of the test section were made up of steel having 0.05 mm thickness [18]. The other two walls and ribs were made of perspex sheet [18]. Fig. 2 shows the computational domain considered for 90^0 broken ribs. The periodic boundary condition was used at the inlet and outlet of the computational domain. One half of the domain was modeled by considering the symmetric condition. In the present study grids were made much finer in the critical regions, such as, near the walls, ribs, separation region and near the reattachment.

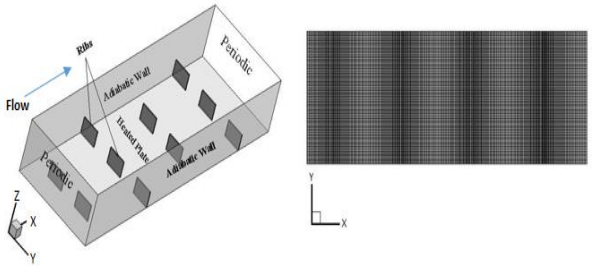


FIGURE 2. Computational domain and grid selection.

MATHEMATICAL MODELING

Numerical simulations were carried out to investigate the heat transfer enhancement in a three-dimensional square channel fitted with different types of ribs. The governing Reynolds-averaged equations for the conservation of mass, momentum and energy equations can be written as

Continuity Equation

$$\frac{\partial\left(\rho\overline{U_i}\right)}{\partial x_i}=0 \tag{1}$$

Momentum Equation

$$\frac{\partial}{\partial x_j}\left(\rho\overline{U}_i\overline{U}_j\right)=-\frac{\partial\overline{P}}{\partial x_i}+\frac{\partial}{\partial x_j}\left[\mu\left(\frac{\partial\overline{U}_i}{\partial x_j}+\frac{\partial\overline{U}_j}{\partial x_i}\right)-\rho\overline{u_i'u_j'}\right] \tag{2}$$

where the term $-\rho\overline{u_i'u_j'}$ in the momentum equation (2) is called the Reynolds stress and its existence here leads to a closure problem.

Energy Equation

$$\rho c_p\overline{U_i}\frac{\partial\overline{T}}{\partial x_i}=k_a\frac{\partial^2\overline{T}}{\partial x_i^2}-\frac{\partial}{\partial x_i}\left(\rho c_p\overline{u_i'T'}\right) \tag{3}$$

where k_a denotes the thermal conductivity of the fluid. The other symbols used here have their usual meanings. To close the system of RANS equations (1) – (3) we have used three turbulence models and these are described in the following section.

Turbulence Models

In the present study the standard k-ε model and its two variants (RNG and realizable models) were used to close the system of governing equations. These models are based on the Boussinesq approximation, which relates the Reynolds stresses to the mean velocity gradients as

$$-\rho\overline{u_i'u_j'}=\mu_t\left(\frac{\partial\overline{U}_i}{\partial x_j}+\frac{\partial\overline{U}_j}{\partial x_i}\right)-\frac{2}{3}\rho\delta_{ij}k \tag{4}$$

here k denotes the Turbulent kinetic energy and is defined as $k=\frac{1}{2}\overline{u_i'u_i'}$, δ_{ij} the Kronecker delta and μ_t the turbulent or eddy viscosity (flow property).

Turbulent transport of temperature or any scalar Φ was modeled in the similar way as that for momentum:

$$-\rho\overline{u_i'\Phi'}=\Gamma_t\left(\frac{\partial\overline{\Phi}}{\partial x_j}\right) \tag{5}$$

The turbulent Prandtl number is defined as the ratio of the eddy viscosity and eddy thermal diffusivity $\mathrm{Pr}_t=\frac{\mu_t}{\Gamma_t}$. A typical value of the turbulent Prandtl number used in engineering computation is approximately 1 [23].

Standard *k-ε* Model. The standard k-ε model is one of the most widely used models. It is a two equation semi-empirical model with one transport equation for turbulent kinetic energy (k) and other for dissipation of turbulent kinetic energy (ε).

The eddy viscosity is modeled as

$$\mu_t=\rho c_\mu {k^2}/{\varepsilon}$$

where C_μ denotes an empirical model constant.

Transport equations for turbulent kinetic energy (k) and its dissipation rate (ε) may be written as

$$\frac{\partial}{\partial \mathrm{x_i}}\left(\rho k\overline{U}_i\right)=\frac{\partial}{\partial \mathrm{x_j}}\left[\left(\mu+\frac{\mu_t}{\sigma_k}\right)\frac{\partial k}{\partial \mathrm{x_j}}\right]+G_k-\rho\varepsilon \tag{6}$$

$$\frac{\partial}{\partial \mathrm{x_i}}\left(\rho\varepsilon\overline{U}_i\right)=\frac{\partial}{\partial \mathrm{x_j}}\left[\left(\mu+\frac{\mu_t}{\sigma_\varepsilon}\right)\frac{\partial\varepsilon}{\partial \mathrm{x_j}}\right]+C_{1\varepsilon}\frac{\varepsilon}{k}\left(G_k\right)-C_{2\varepsilon}\rho\frac{\varepsilon^2}{k} \tag{7}$$

In these equations G_k represents the generation of turbulent kinetic energy due to the mean velocity gradients. The values of the model constants used in these equations

are C_μ = 0.09, $C_{1\varepsilon}$ = 1.44, $C_{2\varepsilon}$ = 1.92, σ_k = 1.0, σ_ε = 1.31 [23].Here σ_ε and σ_k denote the turbulent Prandtl numbers for ε and k, respectively.

RNG *k-ε* Model. The RNG *k-ε* model was derived using the renormalization group theory. The RNG *k-ε* model is similar to the standard *k-ε* model. It has an extra term in its dissipation rate equation that considerably improves the accuracy of swirling and rapidly strained flows [23]. The transport equations for turbulent kinetic energy (k) and dissipation (ε) may be written as

$$\frac{\partial}{\partial x_i}\left(\rho k\bar{U}_i\right) = \mu_t S^2 + \frac{\partial}{\partial x_i}\left(\alpha_k \mu_{\text{eff}} \frac{\partial k}{\partial x_i}\right) - \rho\varepsilon \qquad (8)$$

where $S \equiv \sqrt{2S_{ij}S_{ij}}$, $S_{ij} \equiv \frac{1}{2}\left(\frac{\partial \bar{U}_j}{\partial x_i} + \frac{\partial \bar{U}_i}{\partial x_j}\right)$

$$\frac{\partial}{\partial x_i}\left(\rho\varepsilon\bar{U}_i\right) = C_{1\varepsilon}\left(\frac{\varepsilon}{k}\right)\mu_t S^2 + \frac{\partial}{\partial x_i}\left(\alpha_\varepsilon \mu_{\text{eff}} \frac{\partial \varepsilon}{\partial x_i}\right) - C_{2\varepsilon}\rho\left(\frac{\varepsilon^2}{k}\right) - R \qquad (9)$$

here μ_{eff} denotes the effective viscosity and is written as

$$\mu_{eff} = \mu + \mu_t = \mu + \rho C_\mu \frac{k^2}{\varepsilon}$$

where $\alpha_k, \alpha_\varepsilon, C_{1\varepsilon}, C_{2\varepsilon}$ are derived using the RNG theory.

Realizable *k-ε* Model. The realizable *k-ε* model differs from the standard *k-ε* model in two ways: (a) It has a new formulation for the turbulent viscosity and (b) A new transport equation for the dissipation rate is derived from an exact equation for the transport of the mean square vorticity fluctuations. The transport equations for turbulent kinetic energy (k) and dissipation (ε) may be written as

$$\frac{\partial}{\partial x_i}\left(\rho k\bar{U}_i\right) = \frac{\partial}{\partial x_j}\left[\left(\mu + \frac{\mu_t}{\sigma_k}\right)\frac{\partial k}{\partial x_j}\right] + G_k - \rho\varepsilon \qquad (10)$$

$$\frac{\partial}{\partial x_i}\left(\rho\varepsilon\bar{U}_i\right) = \frac{\partial}{\partial x_j}\left[\left(\mu + \frac{\mu_t}{\sigma_\varepsilon}\right)\frac{\partial \varepsilon}{\partial x_j}\right] + \rho C_1 S_\varepsilon - \rho C_2 \frac{\varepsilon^2}{k + \sqrt{\nu\varepsilon}} \qquad (11)$$

where $C_1 = \max\left[0.43\frac{\eta}{\eta + S}\right]$, $\eta = S\frac{k}{\varepsilon}$

$$S_{ij} = \frac{\bar{U}_{i,j} + \bar{U}_{j,i}}{2}$$

The eddy viscosity is defined as

$$\mu_t = \rho C_\mu \frac{k^2}{\varepsilon}$$

where $C_\mu = \frac{1}{A_0 + A_S\frac{kU^*}{\varepsilon}}$

and $U^* = \sqrt{S_{ij}S_{ij} + \bar{\Omega}_{ij}\bar{\Omega}_{ij}}$

here $\bar{\Omega}_{ij}$ denotes the rate of rotation tensor and A_0 and A_s denote the model constants.

All the governing equations were solved numerically using the finite volume method and the second order upwind scheme was used as the discretization scheme. The SIMPLE (Semi-Implicit Method for Pressure Linked Equations) algorithm was used for the pressure-velocity coupling. The computations were carried out using ANSYS FLUENT 14. We assumed the solutions to be converged for the normalized residual values less than 10^{-5} for all the variables except 10^{-9} for the energy equation.

Three parameters were considered in the present study: Reynolds number (Re), local Nusselt number (Nu_x) and area average Nusselt number (Nu_{av}) and these are defined as $Re = \frac{\rho U d}{\mu}$. The local heat transfer is measured by the local Nusselt number (a quantification of the convective heat transfer taking place at the surface) and is given by $Nu_x = \frac{h_x d}{k_a}$ where $h_x = \frac{q_w}{T_b - T_w}$.

The area average Nusselt number is given by

$$Nu_{av} = \frac{1}{A}\int Nu_x dA$$

The Dittus-Boelter correlation for smooth duct turbulent flow for $Re \geq$ 10,000 with constant heat flux condition is given as $Nu_0 = 0.0243Re^{0.8}Pr^{0.4}$.

RESULTS AND DISCUSSION

Normalized coordinates were used to present various resultsin the present study.The local Nusselt number (Nu) and average Nusselt number (Nu_{av}) were normalized by the Nusselt number (Nu_0) given by Dittus-Boelter correlation. The streamwise coordinate (x) and rib pitch (p) were normalized with the rib height (e) and the spanwise coordinate (z) was normalized by the channel hydraulic diameter (d). Therefore x/e denotes the normalized streamwise coordinate and z/d the normalized spanwise coordinate. Further some other normalized parameters, such as, e/d termed as the blockage ratio and p/e the normalized rib pitch were also used in present study.

The present code was validated with the computational results obtained by Promvonge *et al.* [20]. Fig. 3 shows a comparison of the normalized local Nusselt number for 60^0 V-shaped broken in the streamwise direction and at z/d = 1/4 in the spanwise direction for e/d = 0.0625, s/d = 0.0625 and p/e = 10 with Re of 15000. The variation in the normalized local Nusselt number for the present study is in good agreement with the computational result obtained by Promvonge *et al.* [20] (Fig. 3). In the present study the value of the normalized average Nusselt number obtained for Re= 15000 was 3.96 with a 10 % deviation from the computational result of Promvonge *et al.* [20] and 1.80% deviation from experimental results [18].

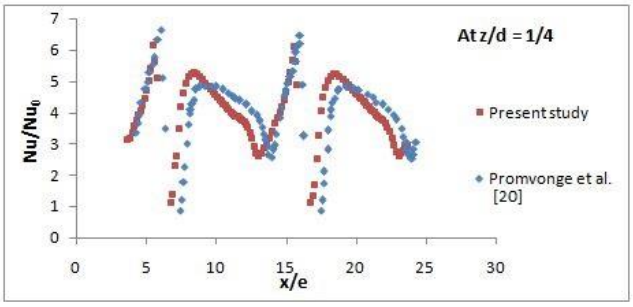


FIGURE 3. Comparison of local Nusselt number with computational study [20] for e/d = 0.0625, p/e = 10 and Re = 15000.

TABLE 1: Average Nusselt number predicted by turbulence models considered for 90^0 attached rib configuration for e/d = 0.15, p/e = 10 and Re = 15000.

S.No.	**Turbulence model**	$\mathbf{Nu_{av}/Nu_0}$
1.	Standard k-ε	2.75
2.	Realizable k-ε	2.69
3.	RNG k-ε	2.71

In order to check the grid independence of the computed results four different meshes with number of elements equal to 152952, 243300, 342500 and 427272 were considered for 90^0 attached ribs. We observed that for the meshes with 342500 and 427272 elements the variation of normalized Nusselt number was negligible. Thus solution using these two fine meshes was considered to be grid independent.

In the present study, the performances of three turbulence models, namely, the standard k-ε model, RNG k-ε model and realizable k-ε model were compared. We observed a small deviation in the predictions of local and average Nusselt number by turbulence models considered (Fig. 4). We also observed from Fig. 4 that the predictions of local Nusselt number by the standard k-ε turbulence models are in good agreement with the experimental data [18] except in the vicinity of the rib. The present predictions of average Nusselt number were in good agreement with the experimental data [18] with maximum 9.56% over-prediction (Table 1) by the turbulence models considered. The standard k-ε model with the enhanced wall treatment was used for all subsequent results reported here.

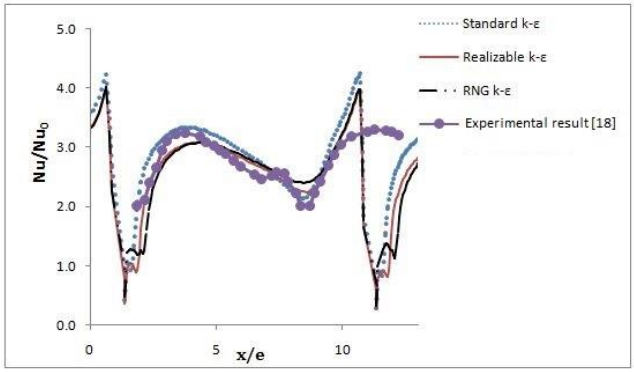


FIGURE 4. Variations of local Nusselt number predicted by different turbulence models.

Fig. 5 shows temperature contours for 90º continuous attached rib. It can be seen from the temperature contours that heat transfer deteriorates immediately after the rib and shows maximum value before each rib. The deterioration of heat transfer after the rib is due to a large recirculation zone formed immediately after the attached rib and thus turbulent kinetic energy decreases (Fig. 6) and hence heat transfer deteriorates.

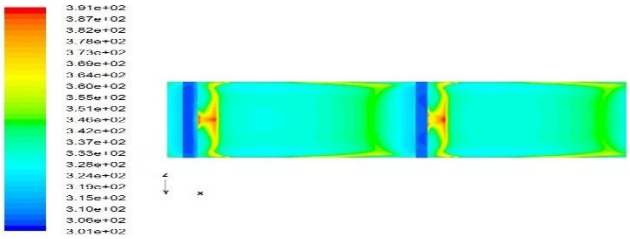


FIGURE 5. Temperature contours on heated plate for continuous attached rib for e/d = 0.15, p/e = 10 and Re = 15000.

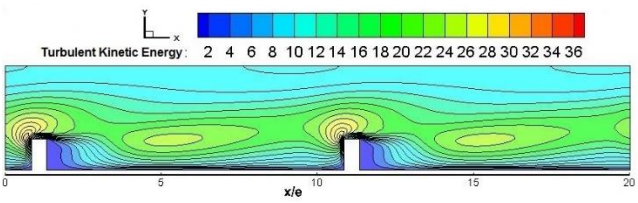


FIGURE 6. Contours of turbulent kinetic energy for 90º continuous attached ribs with e/d = 0.15, p/e = 10 and Re = 15000.

In the case of detached rib configuration the maximum heat transfer takes place in the clearance between the rib and heated plate because of high turbulent kinetic energy (Fig. 7).

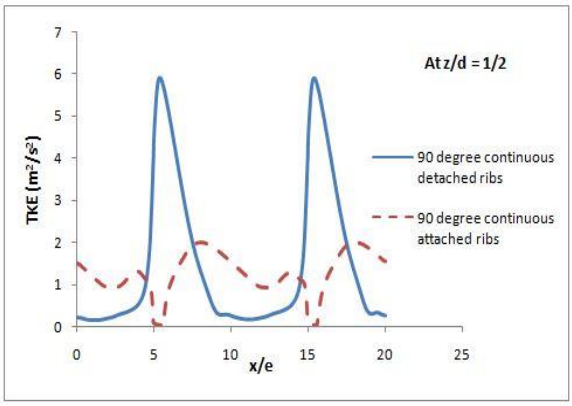


FIGURE 7. Variation of Turbulent kinetic energy for attached and detached 90^0 continuous ribs.

It can be observed from Fig. 7 that the turbulent kinetic energy is high in the vicinity of ribs and wake region for the detached ribs as compared to attached ribs. But after the wake region the turbulent kinetic energy is smaller for the detached rib configuration as compared to that for attached ribs. This behavior is because there is no recirculation after the wake region in the detached ribs and this recirculation region extends up to the reattachment point in the case of attached ribs. Due to this behavior the heat transfer enhancement does not actively take place in the case of detached 90^0 continuous ribs as compared to the attached ribs. The average Nusselt number for attached ribs is found to be more than that for detached ribs for the same configuration (Table 2). For the detached ribs the maximum value of turbulent kinetic energy occurs in the clearance between rib and wall and two counter rotating vortices can be seen after the detached rib (Fig. 9). It can be observed from the temperature contours in Figs. 5 & 8 that the hot spot appearing immediately behind the rib for attached rib case is effectively removed with 90^0 continuous detached rib. This means that the heat transfer deterioration immediately behind the rib in the case of attached solid rib is effectively eliminated with the use of detached ribs.

TABLE 2: Comparison of average Nusselt number for attached and detached rib configurations.

S.No.	Rib configurations	*e/d*	*p/e*	*c/e*	Nu_{av}/Nu_0
1	90^0 continuous attached rib	0.15	10	0	2.75
2	90^0 continuous detached rib	0.15	10	0.5	2.45

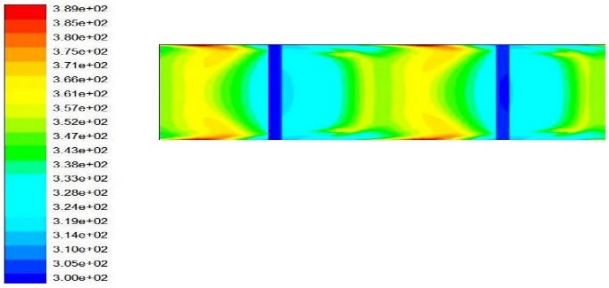


FIGURE 8. Temperature contours for 90º continuous detached ribs with *e/d* = 0.15, *p/e* = 10 and *c/e* = 0.5.

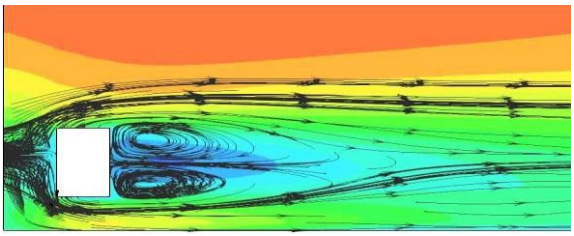


FIGURE 9. Streamtraces for 90º continuous detached ribs with *e/d* = 0.15, *p/e* =10 and *c/e* = 0.5.

Effect of 90^0 Broken Attached Ribs on Heat Transfer

In the present study 90^0 broken attached ribs with blockage ratios (*e/d*) of 0.15, 0.10 and 0.08125 were considered in order to study the effect of blockage ratio on heat transfer augmentation. For each blockage ratio considered two rib configurations were used, i.e., thick ribs (*s/d* = 0.075) and thin ribs (*s/d* = 0.0125) in order to study the effect of rib thickness on heat transfer augmentation. The effect of *Re* varying from 10,000 to 30,000 was also investigated for all blockage ratios and rib thickness considered.

It can be observed from Fig. 10 that the value of the surface Nusselt number is high before the middle region of ribs and side of ribs except in the area close to the side walls shared with side ribs. This behavior is due to the fact that in this region turbulent kinetic energy is high and thus heat transfer is maximum in these regions. However the heat transfer deteriorates immediately after each rib due to flow separation and reattachments.

Broken rib produced higher levels of turbulence over the heated surface due to better mixing of flow. From Fig. 11, it can be observed that the flow is highly disturbed due to broken ribs and the zone of recirculation and reattachment can be observed from streamlines in Fig. 11.

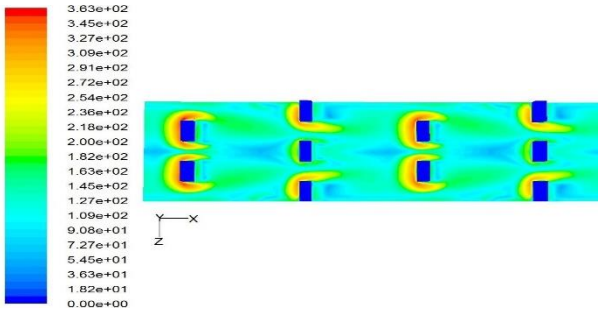


FIGURE 10. Surface Nusselt number contours over the heated plate for 90^0 attached broken thick ribs for e/d = 0.15, p/e = 10 and Re = 15000.

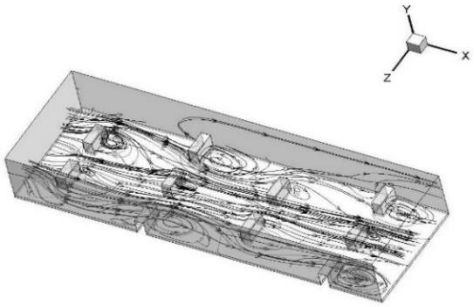


FIGURE 11. Streamtraces for 90^0 broken attached thick ribs for e/d = 0.15, p/e = 10 and Re = 15000.

We can observe from Fig. 12 that the average Nusselt number is high at each Re in case of broken attached ribs as compared to that for continuous attached ribs. Therefore the broken ribs performed well as compared to continuous rib because heat transfer is larger with broken ribs as compared to continuous ribs.

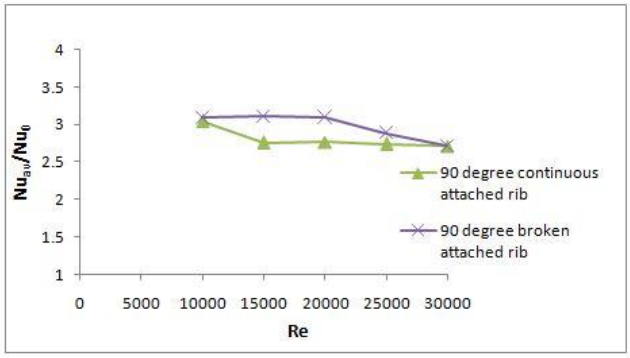


FIGURE 12. Variation of average Nusselt number for 90^0 continuous and broken rib configurations at different Re with e/d = 0.15 and p/e = 10.

Effect of Blockage Ratio and Rib Thickness for 90^0 Broken Rib Configuration on Heat Transfer

It can be observed from Fig. 13 that the local heat transfer is maximum for the blockage ratio of 0.10.

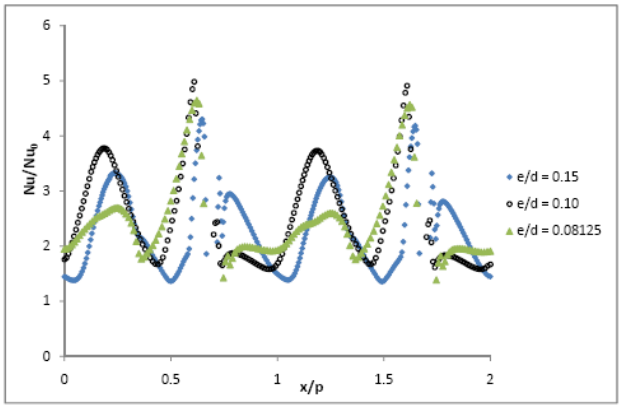


FIGURE 13. Variation of local Nusselt number for 90^0 broken thick ribs for different blockage ratio at z/d = 1/2 for Re = 15000.

In the present study we have investigated the effect of the blockage ratio and for each blockage ratio thick and thin rib configurations were studied. Variation of heat transfer with blockage ratio and rib thickness can be observed in Fig. 14. It can be observed that the heat transfer slightly varies with the blockage ratio for 90^0 broken attached rib.

It can be observed from Fig. 14 that the average Nusselt number slightly decreases with increasing Re. Higher heat transfer can be achieved with thin rib configuration as compared to thick ribs for all rib configurations studied. Here we can also conclude that the ribs with blockage ratio of 0.10 performed slightly better than other blockage ratios with the same value of the rib spacing (p/e= 10).

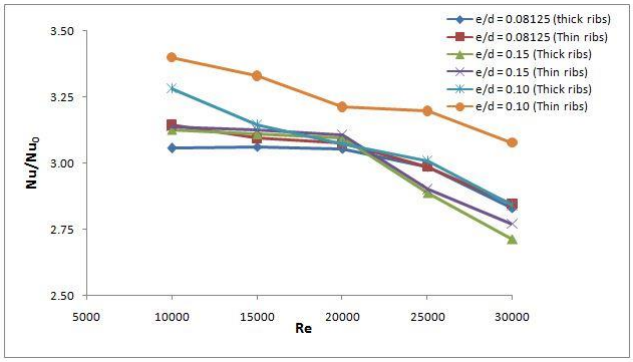


FIGURE 14. Variation of average Nusselt number for different blockage ratios and at different Reynolds numbers for 90^0 broken attached ribs.

CONCLUSION

A computational study was carried out to consider heat transfer augmentation in a three-dimensional square channel fitted using different types of ribs. It was observed that the standard k-ε model provides better results compared to other turbulence models considered. It was observed that thin ribs perform better than thick ribs. Broken ribs

produced high levels of turbulence over the heated surface due to better mixing of flow. The average Nusselt number was found to be more at each Reynolds number in the case of broken attached ribs as compared to the continuous attached ribs. Increasing the Reynolds number provided an adverse effect on heat transfer for all cases. The present results can be used in design of internal cooling passages of advanced gas turbine blades, electronic equipment cooling, solar heaters and many other industrial applications.

ACKNOWLEDGEMENT

The work reported here forms a part of the Department of Science and Technology (DST), Government of India, New Delhi sponsored project (SR/S3/NERC/0114/2012). We gratefully acknowledge the financial support received from DST.

REFERENCES

[1] Han, J.C., and Park, J.S., 1988. "Developing heat transfer in rectangular channel with rib turbulators". Int. J. Heat and Mass Transfer, 31(1), pp. 183-195.

[2] Webb, R.L., Eckert, E.R.G., and Goldstein, R.J., 1971. "Heat transfer and friction in tubes with repeated-rib roughness". Int. J. Heat and Mass Transfer, 14(4), pp. 601-617.

[3] Han, J.C., Glicksman, L.R., and Rohsenow, W.M., 1978. "An investigation heat transfer and friction factor for rib roughened surfaces". Int. J. Heat Mass Transfer, 21(8), pp. 1143-1156.

[4] Sparrow, E.M., and Cur, N., 1982. "Turbulent heat transfer in a symmetrically or asymmetrically heated flat rectangular duct with flow separation at inlet". Trans ASME J. Heat Transfer, 104(1), pp. 82-89.

[5] Han, J.C., 1984. "Heat transfer and friction in channels with two opposite rib roughened walls". Trans ASMEJ. Heat Transfer, 106(4), pp. 774-781.

[6] Han, J.C., Zhang, Y.M., and Lee, C.P., 1991. "Augmented heat transfer in square channels with parallel, crossed, and V-shaped angled ribs". Trans ASMEJ. Heat Transfer, 113(3), pp. 590-596.

[7] Lau, S.C., Kukreja, R. T., and McMillin R. D., 1991. "Effects of V-shaped rib arrays on turbulent heat transfer and friction of fully developed flow in a square channel". Int. J. Heat and Mass Transfer, 34(7), pp. 1605-1616.

[8] Han, J.C., and Zhang Y. M., 1992. "High performance heat transfer ducts with parallel broken and V-shaped broken ribs". Int. J. Heat and Mass Transfer, 35(2), pp. 513-523

[9] Liou, T.M., and Wang, W. B., 1995. "Laser holographic interferometry study of developing heat transfer in a duct with a detached rib arrays". Int. J. Heat and Mass Transfer, 38(1), pp. 91-100.

[10] Rau, G., Cakan, M., Moeller, D., and Arts, T., 1998. "The effect of periodic ribs on the local aerodynamic and heat transfer performance of a straight cooling channel". Trans ASME J. of Turbomachinary, 120(2), pp. 368-375.

[11] Gao, X., and Sunden, B., 2001. "Heat transfer and pressure drop measurements in a rib roughened ducts". Exp. Thermal and Fluid Science, 24(1), pp. 25-34.

[12] Chandra, P.R., Alexander, C.R., and Han, J.C., 2003. "Heat transfer and friction behavior in rectangular channels with varying number of ribbed walls". Int. J. Heat and Mass Transfer, 46(3), pp. 481-495.

[13] Tanda, G., 2004. "Heat transfer in rectangular channels with transfer and V-shaped broken ribs". Int. J. Heat and Mass Transfer, 47(2), pp. 229-243.

[14] Sewall, E.A., Tafti, D.K., Graham, A.B., and Thole, K.A., 2006. "Experimental validation of large eddy simulations of flow and heat transfer in a stationary ribbed duct". Int. J. Heat and Fluid Flow, 27(2), pp. 243-258.

[15] Chang, S.W., Yang, T.L., Huang, R.F., and Sung, K.C., 2007. "Influence of channel height on heat transfer in a rectangular channels with skewed ribs at different bleed conditions". Int. J. Heat and Mass Transfer, 50(23), pp. 4581-4599.

[16] Eiamsa-ard, S., and Promvonge P., 2008. "Numerical study on heat transfer of turbulent channel flow over periodic grooves". Int. Comm. Heat and Mass Transfer, 35(7), pp. 844-852.

[17] Gupta, A., Sri Harsha, V., Prabhu, S.V., and Vedula, R.P., 2008. "Local heat transfer distribution in a square channel with 90^0 continuous, 90^0 saw tooth profiled and 60^0 broken ribs". Exp. Thermal and Fluid Science, 32(4), pp. 997-1010.

[18] SriHarsha, V., Prabhu, S.V., and Vedula R.P., 2009. "Influence of rib height on the local heat transfer distribution and pressure drop in a square channel with 90^0 continuous and 60^0 V-broken ribs". Applied Thermal Engineering, 29(11), pp. 2444-2459.

[19] Tanda, G., 2011. "Effect of rib spacing on heat transfer and friction in a rectangular channel with450 angled rib turbulators on one/two walls". Int. J. Heat and Mass Transfer, 54(5), pp. 1081-1090.

[20] Promvonge, P., Changcharoen, W., Kwankaomeng, S., and Thianpong, C., 2011. "Numerical heat transfer study of turbulent square-duct flow through inline V-shaped discrete ribs". Int. Comm. Heat and Mass Transfer, 38(10), pp. 1392-1399.

[21] Smulsky, Y. L., Terekhov, V. I., and Yarygina, N. I. 2012. "Heat transfer in a turbulent separated flow behind a rib on the surface of square channel at different orientation angles relative to flow direction". Int. J. Heat and Mass Transfer, 55(4): 726-733.

[22] Tang, X., and Zhu, D., 2013. "Flow structure and heat transfer in a narrow rectangular channel with different discrete rib arrays". Chemical Engineering and Processing, 69, pp. 1-14.

[23] Dewan, A., 2011. Tackling Turbulent Flows in Engineering, Springer-Verlag, Heidelberg, Germany.